RSC Advances

PAPER

View Article Online
View Journal | View Issue

Cite this: *RSC Adv.*, 2020, **10**, 7443

Enhanced piezo-photocatalytic performance by piezoelectric and visible light photoexcitation coupling through piezoelectric $Na_{0.5}Bi_{0.5}TiO_3$ micron crystals

Renjie Zhang,[a] Xinyan Wu,[b] Yanqiang Li,[a] Weiquan Shao,[a] Yongcheng Zhang,[a] Zhu Liu,[a] Jiangwu Nie,[c] Jinshan Tan[c] and Wanneng Ye*[ac]

The unique piezoelectric potential of piezoelectrics could lead to performance gains for electrochemical catalysis. Here, a cuboid-like $Na_{0.5}Bi_{0.5}TiO_3$ (NBTO) piezoelectric micron crystal was synthesized by a hydrothermal process. The piezocatalytic and visible light assisted piezo-photocatalytic activities of NBTO were investigated. Surprisingly, under ultrasonic vibration and visible light irradiation, the NBTO exhibited four times faster degradation rate than that under ultrasonic vibration only, although the NBTO doesn't absorb visible light. An efficient coupling between piezoelectric effect and visible light photoexcitation in NBTO was directly demonstrated. The improved piezo-photocatalytic performance is attributed to the piezoelectric potential and the decrease of bandgap of NBTO micron crystal due to strain induced by ultrasonic vibration. A new fundamental mechanism for the improved degradation of organic dye has been proposed for piezoelectric and photoexcitation coupling. This work extends the application of wide band gap piezoelectric materials in the visible light area.

Received 27th December 2019
Accepted 12th February 2020

DOI: 10.1039/d0ra01101k

rsc.li/rsc-advances

1. Introduction

Semiconductor photocatalysts that can directly convert solar energy into chemical energy offers a promising effective route to solve the worsening global environmental pollution and energy crisis, which has received increasing attention in the past few decades.[1–6] Nevertheless, the conversion efficiency of photocatalyst strongly relies on the efficiency of light absorption, the competition of separation and recombination of photoexcited electron–hole pairs, and the efficiency of oxidation–reduction reaction on the surface of photocatalyst.[1,4,5,7] Traditional photocatalysts are more or less subjected to these factors, and thus their photocatalytic efficiency is usually prohibited. To improve the photocatalytic efficiency, strategies such as elemental doping, metal catalyst loading, band gap engineering, surface passivation and heterojunction nanocomposites have been developed recently.[2,7–11] Among these strategies, efficient use of the photoexcited electrons and holes is the crucial motivation. However, the improvement of photocatalytic efficiency for the currently developed photocatalysts is still limited to a certain extent due to the restrictions imposed by material synthesis, material stability and low quantum efficiency.[4–6,11] Therefore, there is still a high desire to look for an effective way to manipulate the photoexcited charge carriers and improve the photocatalytic efficiency of semiconductor photocatalysts.

Besides natural solar energy, mechanical energies such as wind energy, hydroenergy and vibration energy are also amply available in the environment. The application of mechanical energy is another promising choice in the catalysts area. Piezoelectrics are a class of functional materials that could create an electric field (*i.e.* piezoelectric field) within the piezoelectrics in response to mechanical deformation (vibration), such piezoelectric field is created due to the separation between the positive and negative charge centers as the piezoelectric material is strained.[12–17] This piezoelectric field can be directly acted as a natural driving force to promote electrochemical reactions, which could lead to performance gains for electrochemical catalysis, and thus a new concept called piezocatalysis has been developed.[15–27] Different from photocatalysis, the piezoelectric material has the ability to directly convert mechanical energy to chemical energy, which also can be used to mechanically driven water splitting and degradation of organic dye pollutants.[15–27] After the preliminary experiments showed an evolution of H_2 and O_2 by piezoelectric $BaTiO_3$ and ZnO through mechanically vibration,[18] piezocatalytic activities have been extensively demonstrated by various piezoelectric crystals.[15–27] In addition, coupling of piezocatalysis with photocatalysis processes, the catalytic performance can be improved

[a]College of Physics, Qingdao University, Qingdao 266071, China. E-mail: ywn@qdu.edu.cn

[b]College of Electrical Engineering, Qingdao University, Qingdao 266071, China

[c]State Key Laboratory of Bio-Fibers and Eco-Textiles, Qingdao University, Qingdao 266071, China

when the piezoelectric materials were subjected to both mechanical vibration and light irradiation simultaneously. However, either ultraviolet (UV) or sun light was used in these reports due to the fact that all the related piezoelectric materials were wide band gap semiconductors.[28–32] Considering that there are large amounts of visible light in the solar energy reaching earth's surface, if piezocatalysis and visible light driven photocatalysis can be coupled in a single piezoelectric material, which will extend the application of piezoelectric material in the visible light field. Notably, it was reported that when a semiconductor was subjected to a strain, such strain will reduce the symmetry of the material and finally result in significant change in the electronic energy bands.[33,34] Especially, both experimental and theoretical investigations have shown that the bandgaps of semiconductors can be decreased by strain.[35–38] This implies that wide band gap piezoelectric material could absorb long wavelength light (*i.e.* visible light) with the help of strain. Therefore, we are interested in whether visible light could lead to piezocatalysis performance gains when wide band gap piezoelectric material under strain (*i.e.* ultrasonic vibration).

$Na_{0.5}Bi_{0.5}TiO_3$ (NBTO) piezoelectric crystal is a typical semiconductor with wide band gap, large remanent polarization, high Curie temperature and high piezoelectric coefficient.[39,40] In particular, it features excellent chemical stability and high conductivity.[39] In this work, NBTO was synthesized by hydrothermal process, both piezocatalytic and piezo-photocatalytic activities of NBTO were investigated by the degradation of Rhodamine B (RhB) dye. NBTO exhibited high piezocatalytic activity under ultrasonic vibration only. Interestingly, piezo-photocatalytic performance gains were observed under both ultrasonic vibration and visible light irradiation as expected. The working mechanism of coupling the piezocatalytic effect and photoexcitation in NBTO micron crystals has been proposed. It is hoped that our work could understand the mechanism for performance gains in wide band gap piezoelectric material under ultrasonic vibration and light irradiation.

2. Experimental section

2.1 Synthesis of NBTO micron crystals

NBTO sample was synthesized by hydrothermal method. All the chemicals used in this work were analytical purity without further purifications. Firstly, stoichiometric $Bi(NO_3)_3 \cdot 5H_2O$ was dispersed in 30 mL deionized water under magnetic stirring for 1 h at room temperature. After that, an appropriate amount of $C_{16}H_{36}O_4Ti$ was added to the solution under vigorously magnetic stirring for 2 h at 60 °C. Then, an appropriate amount of NaOH solution was slowly dispersed to the above solution to adjust the concentration of NaOH to 15 mol L^{-1}. Finally, after vigorous stirring for 2 h, the suspension solution was transferred to a 40 mL Teflon stainless steel autoclave and heated at 200 °C for 48 h. After natural cooling down to room temperature, the obtained precipitates were filtered and washed with distilled water for five times. The final products were collected after drying in a dry box at 80 °C for 10 h.

2.2 Materials characterizations

The crystal structure of sample was determined by powder X-ray diffraction (XRD) with Cu K_α ($\lambda_{K\alpha}$ = 0.154186 nm) (Rigaku SmartLab diffractometer). The morphology and microstructure were investigated by scanning electron microscopy (SEM, ZEISS, Sigma 500) and transmission electron microscopy (TEM, JEOL JEM 2100F) operated at 200 kV. Energy dispersive X-ray spectroscopy (EDX) was used to analyze the elemental composition of the sample. X-ray photoelectron spectroscopy (XPS) was carried out on an Escalab 250Xi spectrometer with an Al-Kα (1486.6 eV) (ThermoFisher Scientific, USA). The ultraviolet-visible (UV-vis) diffuse reflectance spectrum was measured using an UV-vis spectrophotometer (Shimadzu, UV-2450) in the wavelength range of 200–800 nm with $BaSO_4$ as a reference.

2.3 Photo-/piezocatalytic activities evaluation

The photo-/piezocatalytic performances of the NBTO sample were evaluated by the degradation of RhB dye (major absorption peak at 554 nm). The visible light was supplied by a 500 W xenon lamp equipped with a 420 nm cutoff filter. An ultrasonic cleaner with a power of 120 W and a frequency of 40 kHz was used to apply periodic local mechanical strain to the sample. Briefly, 0.2 g sample was dispersed to 50 mL of 10 mg L^{-1} RhB aqueous solution. Prior to visible light irradiation and ultrasonic vibration, the mixture solution was magnetically stirred in the dark for 30 min aimed to achieve an adsorption–desorption equilibrium between RhB and sample. The RhB concentration after equilibration was denoted as the initial concentration (C_0). Subsequently, the mixture solution was exposed to visible light irradiation or ultrasonic vibration under magnetic stirring. In the degradation process, after every 20 min, 4 mL of the above suspension was collected and then centrifuged, the residual concentrations (C_t) of RhB at the degradation time t was measured using UV-vis spectrophotometer around the wavelength of 554 nm and plotted as a function of degradation time. The percentage of residual concentrations of RhB was indicated as C_t/C_0. To test the stability of the sample, the tested samples were collected and repeated the catalytic process for three times under the same experimental conditions.

3. Results and discussion

3.1 Structure, elemental distribution and morphology

Fig. 1 shows powders XRD θ–2θ pattern of NBTO sample. All the observed diffraction peaks can be indexed according to the monoclinic structure of NBTO (JCPDS card no. 46-0001). No other diffraction peaks can be detected within the limit of the instrument sensitivity, indicating that the obtained sample is desired single-phase compound. The lattice parameters were calculated to be a = 5.537 Å, b = 6.682 Å and c = 5.513 Å, which are consistent with the standard values of NBTO.

XPS investigations were used to check the surface chemical states and elemental compositions of the NBTO sample, as shown in Fig. 2. Fig. 2(a) displays the entire XPS spectrum of the sample. Besides weak C 1s peak due to carbon tape, all desired elements of Na, Bi, Ti and O were detected, confirming that the

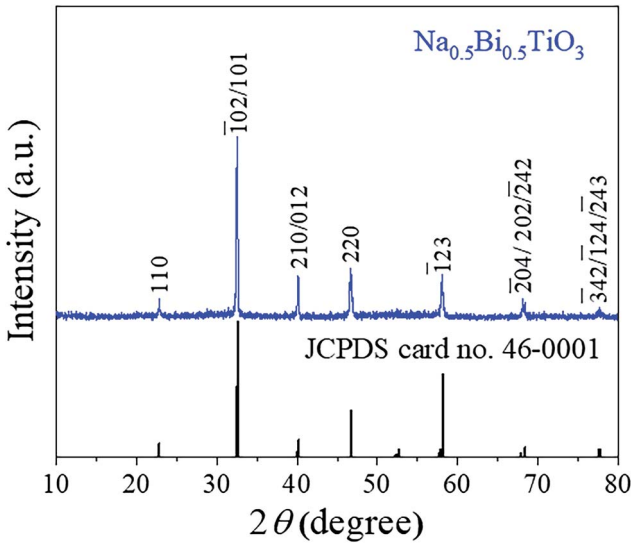

Fig. 1 X-ray diffraction pattern of $Na_{0.5}Bi_{0.5}TiO_3$ powder sample.

as-prepared sample consists of Na, Bi, Ti and O elements. Fig. 2(b)–(f) give the high resolution XPS spectra for Na 1s, Bi 4f, Ti 2p, O 1s and C 1s, the binding energies for the former four elements are calibrated with the C 1s peak (284.6 eV). Fig. 2(b) shows the Na 1s spectrum of the NBTO sample. The binding energy peak located at 1070.75 eV attributes to Na^+ ions in the sample.[41] Fig. 2(c) reveals the Bi 4f spectrum, where two characteristic binding energy peaks located at 158.85 eV (Bi $4f_{7/2}$) and 164.15 eV (Bi $4f_{5/2}$) correspond to Bi^{3+} chemical state in the sample.[42] The Ti 2p spectrum is provided in Fig. 2(d), where two main peaks at 457.85 eV and 464.05 eV are ascribed to the Ti $2p_{3/2}$ and Ti $2p_{1/2}$ transitions, respectively. It indicates that Ti ions in the sample are Ti^{4+} chemical state.[43] Fig. 2(e) displays the O 1s spectrum which could be fitted with two Gaussian-resolved peaks. The main peak located at 529.4 eV corresponds to lattice oxygen O_2^- ions in the NBTO sample. The weak peak at 530.95 eV probably results from the surface hydroxyl groups under the effect of hydroxylation due to the samples are usually exposed to ambient atmosphere.[44] The XPS investigations and the XRD result confirm that the as-prepared NBTO sample is single-phase compound.

The morphology and elemental distribution of the NBTO were observed by SEM and EDX elemental mapping images, as shown in Fig. 3. The product exhibits cuboid-like morphology and the diagonal length of these cuboids range from 0.6 to 2.5 μm, as displayed in Fig. 3(a). Fig. 3(c)–(f) display the EDX elemental mapping images of an individual cuboid-like crystal (Fig. 3(b)), confirming that the Na, Bi, Ti and O elements are uniformly distributed in the cuboid-like crystal. According to EDX measurement, semi-quantitative elemental analysis reveals that the atomic ratio of Na : Bi : Ti : O is 9.76 : 10.09 : 18.16 : 61.99, which is very close to the theoretical stoichiometric ratio of NBTO.

The microstructure of the cuboid-like NBTO crystal was further observed by TEM. Fig. 4(a) shows a typical TEM image of two NBTO cuboids. Fig. 4(b) is a typical selected-area electron diffraction (SAED) pattern and Fig. 4(c) is the corresponding high-resolution TEM (HRTEM) image. Both of them were taken from the cuboid-like crystal indicated with a red dotted circle in Fig. 4(a). The SAED pattern shown in Fig. 4(b) can be indexed as [$2\bar{2}1$] of monoclinic-structured NBTO. The SAED pattern

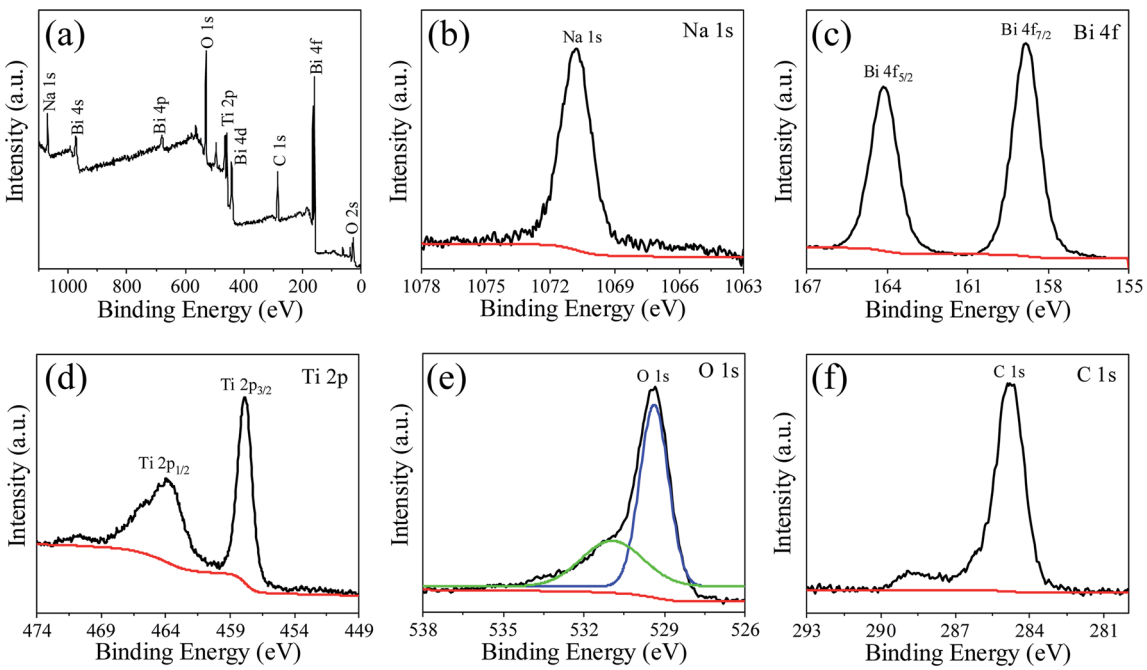

Fig. 2 XPS spectra for $Na_{0.5}Bi_{0.5}TiO_3$ of (a) survey scan, (b) Na 1s spectrum, (c) Bi 4f spectrum, (d) Ti 2p spectrum, (e) O 1s spectrum and (f) C 1s spectrum.

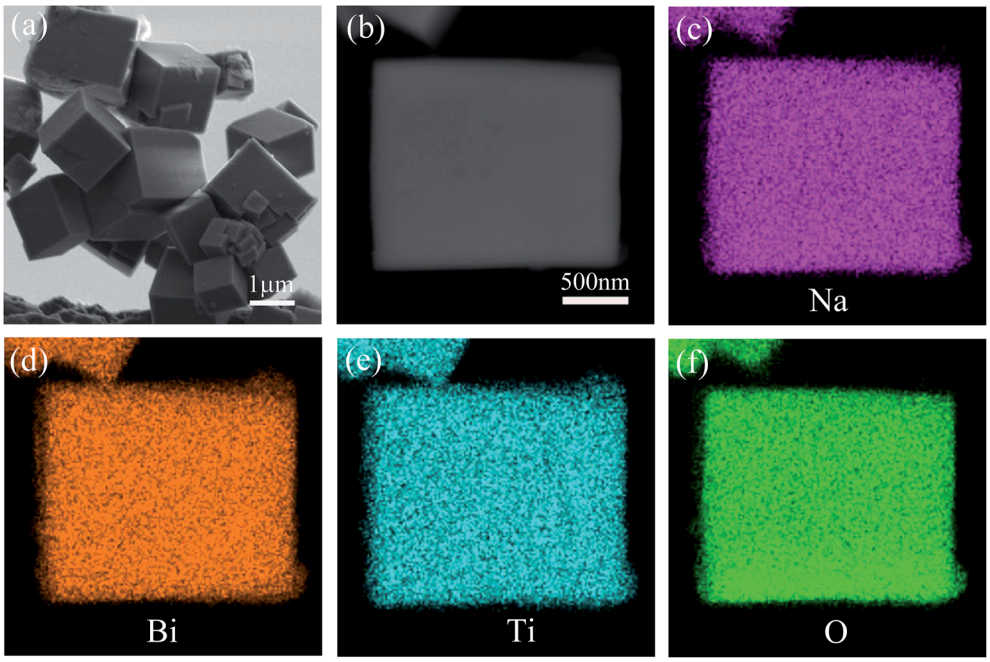

Fig. 3 (a) SEM image of NBTO. (c)–(f) EDX elemental mapping images of a single $Na_{0.5}Bi_{0.5}TiO_3$ micron cuboid shown in (b).

exhibits regular and sharp diffraction spots, demonstrating the single crystal nature of the cuboid-like crystal. In the HRTEM image of Fig. 4(c), the two crystalline planes with lattice spacings are about 0.394 and 0.279 nm and make an angle of ~88.65°, corresponding to the (110) and ($\bar{1}$02) planes of NBTO. In fact, many cuboid-like crystals were rotated in our TEM observation. The contrast of grain boundary or defect was not observed, confirming that these cuboid-like crystals are single crystal.[45]

3.2 Optical properties, piezo-/photocatalytic performance

The UV-vis diffuse reflectance absorption spectrum of the NBTO sample was measured to determine its optical band gap energy (E_g), as shown in Fig. 5. The estimated E_g value of the present

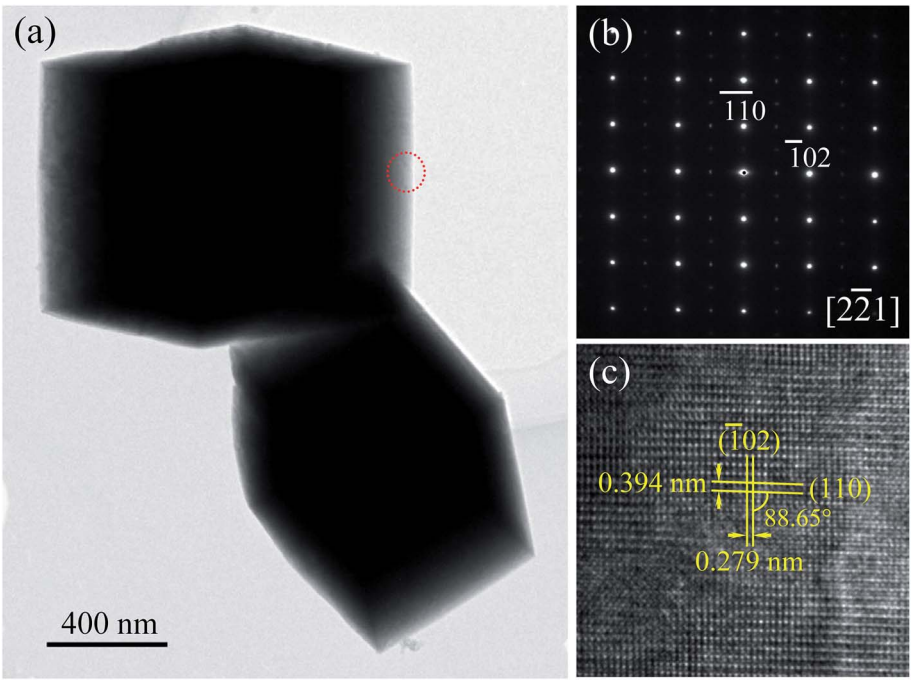

Fig. 4 (a) TEM image of $Na_{0.5}Bi_{0.5}TiO_3$. (b) SAED pattern and (c) the corresponding HRTEM image recorded from the area marked with a red dotted circle in (a).

NBTO sample is ~3.14 eV (inset of Fig. 5), according to the plot of $(\alpha h\nu)^2$ as a function of photon energy $h\nu$ using Tauc's equation.[46] This E_g value is very close to the previously reported values of bulk NBTO.[47,48] The optical properties demonstrate that the NBTO sample is a wide band gap semiconductor and almost can not response to visible light. The piezo-/photocatalytic performances of the NBTO sample were evaluated by the degradation of RhB solution under different reaction conditions: (i) visible light irradiation, (ii) ultrasonic vibration, and (iii) both ultrasonic vibration and visible light irradiation. The degradation efficiency curves are exhibited in Fig. 6(a), meanwhile, the corresponding plots of $\ln(C_0/C_t)$ *versus* reaction time showing rate constant k values are displayed in Fig. 6(b). As provided in Fig. 6(a), in the absent of NBTO catalyst, the self-degradation of RhB dye can be negligible under both ultrasonic vibration and visible light irradiation after 180 min. When the NBTO was used as catalyst just under visible light irradiation only, except weak absorption (4%), almost no degradation reaction was observed within 180 min. These results directly confirm that the NBTO can not absorb visible light as revealed by the UV-vis diffuse reflectance absorption spectrum measurement. However, 59% of the RhB dye in the solution was degraded by NBTO under ultrasonic vibration only after the same time, demonstrating that the present NBTO sample has obvious piezocatalytic activity. Surprisingly, the degradation efficiency can be significantly improved when both ultrasonic vibration and visible light irradiation were applied to the NBTO simultaneously, the finally degradation efficiency reached as high as 98% in the same time. Obviously, by combining ultrasonic vibration and visible light irradiation, the NBTO sample exhibits four times faster degradation rate (k of 0.01855 min^{-1}) than that under ultrasonic vibration (k of 0.00436 min^{-1}) only, as shown in Fig. 6(b). Visible light assisted piezo-photocatalytic effect was directly demonstrated by NBTO micron crystals, although NBTO can not response to visible light under static condition. The mechanism for the enhanced piezo-photocatalytic performance will be discussed below. Note that this finding is very important for extending the applications of piezoelectric catalysts in the long-wavelength field.

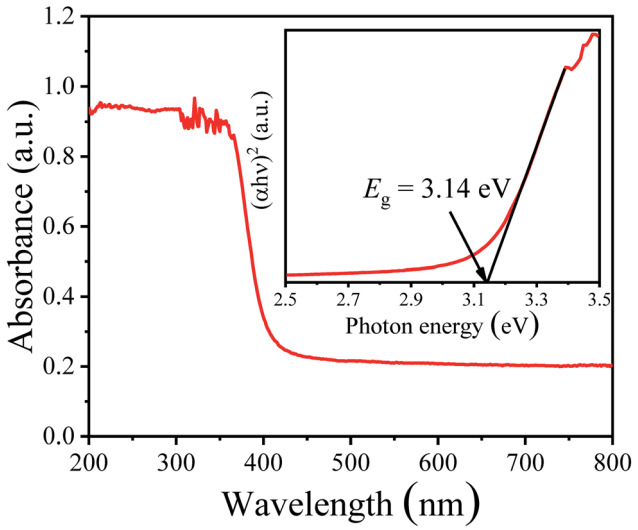

Fig. 5 UV-vis diffuse reflectance absorption spectrum and the inset is the plot of $(\alpha h\nu)^2$ as a function of the photon energy $h\nu$ around the absorption edge of $Na_{0.5}Bi_{0.5}TiO_3$ sample.

To investigate the role of the reactive species in the piezo-photocatalytic process, trapping experiments were designed and performed by purposefully introducing different scavengers into the reaction solution. Fig. 6(c) shows the effects of different scavengers on the piezo-photocatalytic efficiency of the NBTO, meanwhile, the corresponding plots of $\ln(C_0/C_t)$ *versus* reaction time showing rate constant k values are displayed in Fig. 6(d). Notably, the piezo-photocatalytic efficiency of the NBTO decreases slightly after the addition of disodium ethylenediaminetetraacetate (EDTA-2Na, 2 mM, h^+ scavenger), while it is obviously inhibited by the addition of *tert*-butyl alcohol (TBA, 2 mM, ·OH scavenger) and benzoquinone (BQ, 0.5 mM, $\cdot O_2^-$ scavenger) in the reaction solution. These results directly demonstrate that both ·OH and $\cdot O_2^-$ active oxidative species are *in situ* generated and responsible for the degradation of RhB.

To explore the reusability of the NBTO catalysts, three recycling experiments were evaluated with each reaction fixed for 180 min under ultrasonic vibration and visible light irradiation, as displayed in Fig. 7(a). After three consecutive recycling processes, the degradation efficiency declines from about 100% to 80%. Two possibly reasons account for such decline, one is the loss of the catalyst during the recycling experiments; the other is the fatigue of the catalyst. During the recycling catalytic process, the ferroelectric polarization value might decline due to the well-known ferroelectric polarization fatigue,[49] which results in the decreasing of the piezoelectric field, and thus the degradation efficiency declined due to the charges separation efficiency decreased. Fig. 7(b) shows the morphology of the NBTO catalyst after three cycle tests. No evident change of the morphology was observed. In addition, from its SAED pattern shown in the inset of Fig. 7(b), the crystal structure of the NBTO micron crystal was also unchanged, indicating that the NBTO micron crystals are very stable in piezo-photocatalytic reaction process.

3.3 Piezo-/photocatalytic mechanism

The piezocatalysis mechanism of NBTO micron crystals is illustrated in Fig. 8(a). When the NBTO micron crystals were subjected to compression stress induced by ultrasonic wave, such stress leaded the deformation of NBTO micron crystals, and thus a piezoelectric field (piezo-E) was created within the NBTO micron crystal due to the separation between the positive and negative charge centers. It is known that the occurrence of piezocatalysis is strongly related to free charges in the piezoelectric material, because the existence of free charges may largely reduce the activation energy to drive these charges transfer to the reaction surface of catalyst.[17,22,24,26] For the present NBTO micron crystals, it is reasonable that it contains free charges due to defects in the crystal. Thus, the piezo-E promoted these free charges to migrate to the surfaces of these micron crystals. At this moment, these separated free charges

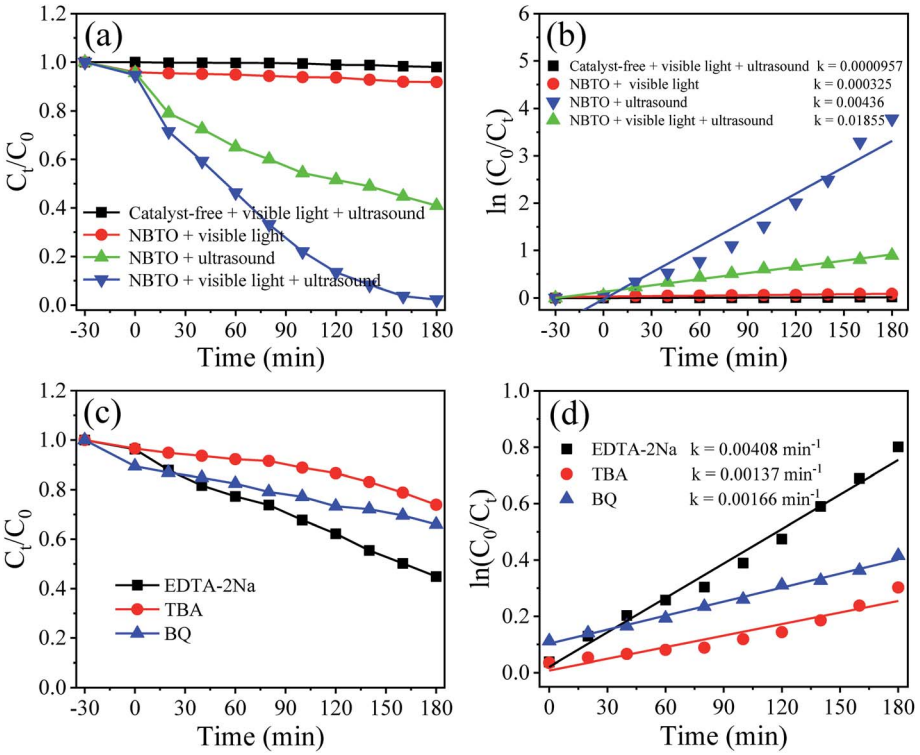

Fig. 6 (a) Degradation efficiency curves of $Na_{0.5}Bi_{0.5}TiO_3$ on the degradation of RhB solution under different reaction conditions and (b) corresponding plots of $\ln(C_0/C_t)$ *versus* reaction time. (c) Active species trapping degradation experiments for $Na_{0.5}Bi_{0.5}TiO_3$ under simultaneous ultrasonic vibration and visible light irradiation on the degradation of RhB and (d) corresponding $\ln(C_0/C_t)$ *versus* reaction time with various scavengers.

did not react with hydroxyl groups and O_2 during the compression process as those free charges were shackled by the piezo-*E*. When the NBTO micron crystals were free of stress, the piezo-*E* disappeared and those separated free charges were free indeed. Then, the electrons reacted with the dissolved O_2 in the reaction solution to yield $\cdot O_2^-$, while the holes were finally trapped by OH^- at the surface of the crystals to form $\cdot OH$ radicals. Finally, these radicals oxidized RhB dye molecules in the aqueous solution, generating eco friendly CO_2 and H_2O.

In the piezocatalysis process, the following chemical reaction processes occurred:[50]

NBTO micron crystals + ultrasonic vibration (compression) → deformation of NBTO micron crystals → separation of positive and negative charge centers → piezo-*E* → separation of charges (free e^- and free h^+).

When the NBTO micron crystals were free of stress during periodic mechanical vibrations,

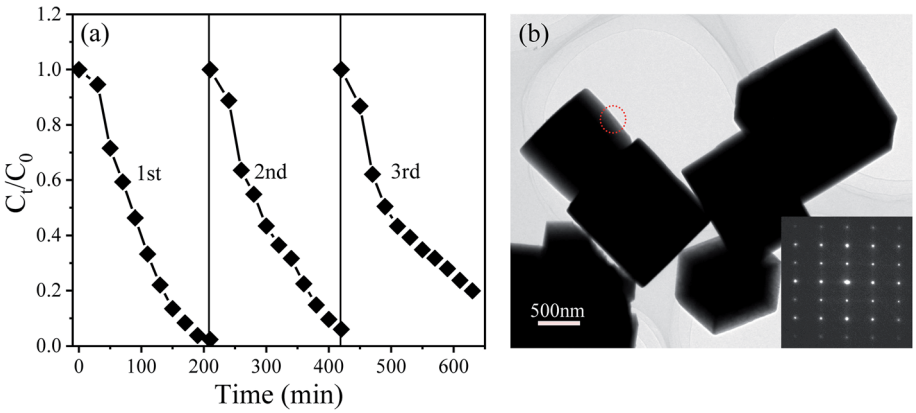

Fig. 7 (a) The cycling performance of the $Na_{0.5}Bi_{0.5}TiO_3$ for the degradation of RhB under both ultrasonic vibration and visible light irradiation. (b) TEM image of the cycling used catalyst and the inset is a SAED pattern recorded from the area marked with a red dotted circle.

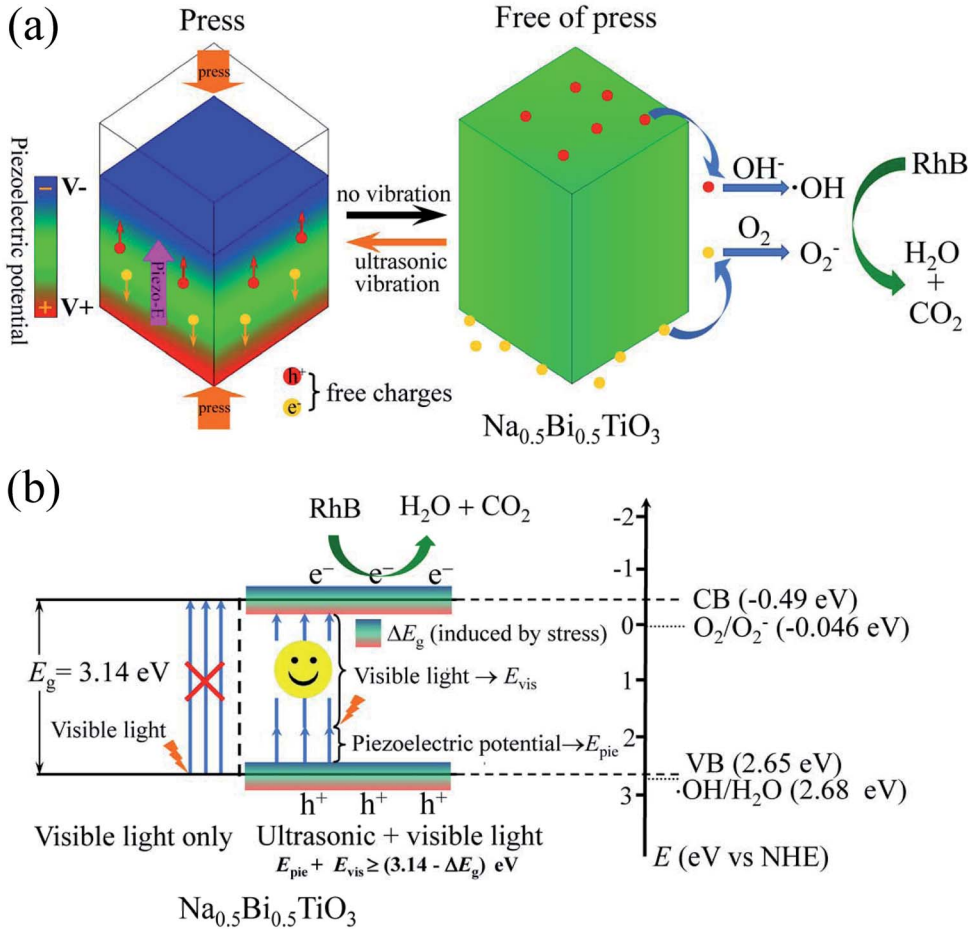

Fig. 8 (a) Schematic diagrams showing the piezocatalytic mechanism of $Na_{0.5}Bi_{0.5}TiO_3$ under ultrasonic vibration. (b) Proposed working mechanism for piezo-photocatalytic of $Na_{0.5}Bi_{0.5}TiO_3$ under both ultrasonic vibration and visible light irradiation.

$$e^- + O_2 \rightarrow \cdot O_2^-,$$

$$h^+ + OH^- \rightarrow \cdot OH,$$

$$RhB + \cdot O_2^-/\cdot OH \rightarrow CO_2 + H_2O$$

When the NBTO micron crystals were subjected to ultrasonic vibration and visible light irradiation simultaneously, the piezo-photocatalytic mechanism of NBTO is schematically shown in Fig. 8(b). Besides the above mentioned piezocatalysis process, the possibility of visible light assisted piezo-photocatalytic process is explained as follows. Considering that the band gap of the present NBTO micron crystals is 3.14 eV, the electrons in the valence band can not be excited to the conduction band by visible light only because the energy (E_{vis}) provided by visible light is too low. However, when the NBTO micron crystals were subjected to ultrasonic vibration and visible light simultaneously, two reasons might account for the visible light absorption by NBTO micron crystals. Firstly, the produced piezo-*E* within the NBTO micron crystals can promote the potential energy (E_{pie}) of these electrons in the valence band. Secondly, strain engineering investigations have demonstrated that the electronic energy bands of semiconductors can be significant changed by external strain.[33,34] Take $(FAPbI_3)_{0.85}$-$(MAPbBr_3)_{0.15}$,[35] $KNbO_3$,[36] $BiFeO_3$ (ref. 37) and ZnO[38] as examples, either experimental or theoretical investigations have demonstrated that their electronic band structure could be changed on account of the strain, contributing to a narrowed bandgap. Similarly, the band gap of the present NBTO micron crystal could more or less decreased (ΔE_g represents the decreased value) due to the strain derived from the ultrasonic vibration. The effect of strain on the bandgap of NBTO will be further investigated. If the sum of the value of $E_{vis} + E_{pie}$ was larger than $(3.14 - \Delta E_g)$ eV, the electrons in the valence band could be photoexcited to the conduction band, and an equal number of holes were left on the valence band. In addition, the piezo-*E* within the micron crystals could also act as a driving force to promote the photogenerated electron/hole pairs to migrate to the surfaces of these micron crystals in the opposite directions and thus reduce their recombination rate.[13,16,28] Thus, more electron/hole pairs could be produced in the piezo-photocatalytic process compared with the single piezocatalytic process which increases the quantities of $\cdot OH$ and $\cdot O_2^-$

radicals, resulting in higher degradation efficiency in the degradation of RhB dye.

4. Conclusions

The piezo-photocatalyst NBTO micron crystals were synthesized by hydrothermal process. The as-prepared NBTO sample displayed high piezocatalytic activity under ultrasonic vibration only. More importantly, although NBTO can not absorb visible light due to its wide band gap, it exhibited four times faster degradation rate under ultrasonic vibration and visible light irradiation than that under ultrasonic vibration only. Visible light assisted piezo-photocatalytic effect was directly demonstrated by NBTO micron crystals. The improved piezo-photocatalytic performance is attributed to the piezoelectric potential and the decrease of bandgap of NBTO micron crystal due to strain induced by the ultrasonic vibration. The piezoelectric potential can promote the separation of photogenerated charge carriers, which increases the quantities of $\cdot OH$ and $\cdot O_2^-$ radicals, resulting in enhanced degradation efficiency in the degradation of RhB dye. This work may be extended to other piezocatalytic systems and offers a new option for designing high-performance piezoelectric catalysts for pollutant treatment.

Conflicts of interest

There are no conflicts of interest.

Acknowledgements

This work was supported by the National Science Foundation of China (11674186, 11504193) and the innovation experiment project of Qingdao University.

References

1 W. J. Wang, G. Y. Li, D. H. Xia, T. C. An, H. J. Zhao and P. K. Wong, *Environ. Sci.: Nano*, 2017, **4**, 782–799.
2 C. Xu, P. R. Anusuyadevi, C. Aymonier, R. Luque and S. Marre, *Chem. Soc. Rev.*, 2019, **48**, 3868–3902.
3 S. Bolisetty, M. Peydayesh and R. Mezzenga, *Chem. Soc. Rev.*, 2019, **48**, 463–487.
4 A. Polman, M. Knight, E. C. Garnett, B. Ehrler and W. C. Sinke, *Science*, 2016, **352**, aad4424.
5 J. Liu, Y. Liu, N. Y. Liu, Y. Z. Han, X. Zhang, H. Huang, Y. Lifshitz, S. T. Lee, J. Zhong and Z. H. Kang, *Science*, 2015, **347**, 970–974.
6 J. H. Kim, D. Hansora, P. Sharma, J.-W. Jang and J. S. Lee, *Chem. Soc. Rev.*, 2019, **48**, 1908–1971.
7 R. Marschall, *Adv. Funct. Mater.*, 2014, **24**, 2421–2440.
8 I. Grinberg, D. V. West, M. Torres, G. Y. Gou, D. M. Stein, L. Y. Wu, G. N. Chen, E. M. Gallo, A. R. Akbashev, P. K. Davies, J. E. Spanier and A. M. Rappe, *Nature*, 2013, **503**, 509–512.
9 X. G. Zhang, X. B. Ke and J. F. Yao, *J. Mater. Chem. A*, 2018, **6**, 1941–1966.
10 R. Liu, Z. Zheng, J. Spurgeon and X. G. Yang, *Energy Environ. Sci.*, 2014, **7**, 2504–2517.
11 Z. Q. Zhang, L. L. Bai, Z. J. Li, Y. Qu and L. Q. Jing, *J. Mater. Chem. A*, 2019, **7**, 10879–10897.
12 X. Wang, J. Zhou, J. Song, J. Liu, N. Xu and Z. L. Wang, *Nano Lett.*, 2006, **6**, 2768–2772.
13 Z. L. Wang, *Nano Today*, 2010, **5**, 540–552.
14 Z. L. Wang, W. Z. Wu and C. Falconi, *MRS Bull.*, 2018, **43**, 922–927.
15 M. B. Starr, J. Shi and X. D. Wang, *Angew. Chem., Int. Ed.*, 2012, **51**, 5962–5966.
16 M. B. Starr and X. D. Wang, *Nano Energy*, 2015, **14**, 296–311.
17 X. D. Wang, G. S. Rohrer and H. X. Li, *MRS Bull.*, 2018, **43**, 946–951.
18 K. S. Hong, H. F. Xu, H. Konishi and X. C. Li, *J. Phys. Chem. Lett.*, 2010, **1**, 997–1002.
19 J. Shi, M. B. Starr, H. Xiang, Y. Hara, M. A. Anderson, J. H. Seo, Z. Q. Ma and X. D. Wang, *Nano Lett.*, 2011, **11**, 5587–5593.
20 H. Lin, Z. Wu, Y. M. Jia, W. J. Li, R.-K. Zheng and H. S. Luo, *Appl. Phys. Lett.*, 2014, **104**, 162907.
21 J. M. Wu, W. E. Chang, Y. T. Chang and C. K. Chang, *Adv. Mater.*, 2016, **28**, 3718–3725.
22 Y. Feng, L. Ling, Y. Wang, Z. Xu, F. Cao, H. Li and Z. Bian, *Nano Energy*, 2017, **40**, 481–486.
23 H. You, X. Ma, Z. Wu, L. Fei, X. Chen, J. Yang, Y. Liu, Y. Jia, H. Li, F. Wang and H. Huang, *Nano Energy*, 2018, **52**, 351–359.
24 J. Wu, N. Qin and D. Bao, *Nano Energy*, 2018, **45**, 44–51.
25 Z. Liang, C.-F. Yan, S. Rtimi and J. Bandara, *Appl. Catal., B*, 2019, **241**, 256–269.
26 C. Jin, D. Liu, J. Hu, Y. Wang, Q. Zhang, L. Lv and F. Zhuge, *Nano Energy*, 2019, **59**, 372–379.
27 D. Liu, Y. Song, Z. Xin, G. Liu, C. Jin and F. Shan, *Nano Energy*, 2019, **65**, 104024.
28 X. Xue, W. Zang, P. Deng, Q. Wang, L. Xing, Y. Zhang and Z. L. Wang, *Nano Energy*, 2015, **13**, 414–422.
29 H. Li, Y. Sang, S. Chang, X. Huang, Y. Zhang, R. Yang, H. Jiang, H. Liu and Z. L. Wang, *Nano Lett.*, 2015, **15**, 2372–2379.
30 S. Singh and N. Khare, *Nano Energy*, 2017, **38**, 335–341.
31 Y.-L. Liu and J. M. Wu, *Nano Energy*, 2019, **56**, 74–81.
32 D. Yu, Z. Liu, J. Zhang, S. Li, Z. Zhao, L. Zhu, W. Liu, Y. Lin, H. Liu and Z. Zhang, *Nano Energy*, 2019, **58**, 695–705.
33 I. Goroff and L. Kleinman, *Phys. Rev.*, 1963, **132**, 1080–1084.
34 F. H. Pollak and M. Cardona, *Phys. Rev.*, 1968, **172**, 816–837.
35 C. Zhu, X. Niu, Y. Fu, N. Li, C. Hu, Y. Chen, X. He, G. Na, P. Liu, H. Zai, Y. Ge, Y. Lu, X. Ke, Y. Bai, S. Yang, P. Chen, Y. Li, M. Sui, L. Zhang, H. Zhou and Q. Chen, *Nat. Commun.*, 2019, **10**, 815.
36 R. P. Tiwari, B. Birajdar and R. K. Ghosh, *J. Phys.: Condens. Matter*, 2019, **31**, 505502.
37 H. Dong, Z. Wu, S. Wang, W. Duan and J. Li, *Appl. Phys. Lett.*, 2013, **102**, 072905.
38 Z. Xu, Q. Hou, F. Guo, Y. Li and C. Li, *Comput. Mater. Sci.*, 2019, **169**, 109120.

39 C. J. He, Y. G. Zhang, L. Sun, J. M. Wang, T. Wu, F. Xu, C. L. Du, K. J. Zhu and Y. W. Liu, *J. Phys. D: Appl. Phys.*, 2013, **46**, 245104.
40 Z. Zhu, J. Li, S. Li and C. Li, *Ceram. Int.*, 2019, **45**, 17495–17501.
41 Z. Q. Guo, N. X. Miao, J. P. Zhou, Y. X. Lei, Q. Ul Hassan and M. M. Zhou, *J. Mater. Chem. A*, 2017, **5**, 17589–17600.
42 W. Morgan, W. Stec and J. Van Wazer, *Inorg. Chem.*, 1973, **12**, 953–955.
43 J. Hou, R. Cao, Z. Wang, S. Jiao and H. Zhu, *J. Mater. Chem.*, 2011, **21**, 7296–7301.
44 M. A. Peck and M. A. Langell, *Chem. Mater.*, 2012, **24**, 4483–4490.
45 L. H. Wang, J. Teng, P. Liu, A. Hirata, E. Ma, Z. Zhang, M. W. Chen and X. D. Han, *Nat. Commun.*, 2014, **5**, 4402.
46 J. Tauc, R. Grigorovici and A. Vancu, *Phys. Status Solidi B*, 1966, **15**, 627–637.
47 H. Q. Sun, Q. W. Zhang, X. S. Wang and Y. Zhang, *Ceram. Int.*, 2014, **40**, 15669–15675.
48 G. Cilaveni, K. V. Ashok Kumar, S. S. K. Raavi, Ch. Subrahmanyam and S. Asthana, *J. Alloys Compd.*, 2019, **798**, 540–552.
49 Y. A. Genenko, J. Glaum, M. J. Hoffmann and K. Albe, *Mater. Sci. Eng., B*, 2015, **192**, 52–82.
50 K. S. Hong, H. F. Xu, H. Konishi and X. C. Li, *J. Phys. Chem. C*, 2012, **116**, 13045–13051.